Current Optics and Photonics
Vol. 3, No. 5, October 2019, pp. 374-381

ISSN: 2508-7266(Print) / ISSN: 2508-7274(Online)
DOI: https://doi.org/10.3807/COPP.2019.3.5.374

An Optical Cavity Design for an Infrared Gas Detector Using an Off-axis Parabolic Mirror

You-Jin Jeong[1], Dong-Hwa Kang[1], Jae-Yeong Seo[1], Ye-Ji Jo[1], Jin-Hee Seo[1], Hwan-Young Choi[2], and Mee-Suk Jung[1]*

[1]Department of Nano-optical Engineering, Korea Polytechnic University, Siheung 15073, Korea
[2]School of Mechatronics Engineering, Korea University of Technology and Education, Cheonan 31253, Korea

(Received June 24, 2019 : revised July 29, 2019 : accepted July 30, 2019)

This study examined a method for designing the optical cavity of a non-dispersive infrared gas detector. The infrared gas detector requires an optical cavity design to lengthen the ray path. However, the optical cavity with multiple reflecting surfaces has off-axis aberration due to the characteristics of the reflecting optical system. The rays were parallelized by using the off-axis parabolic mirror to easily increase the ray path and eliminate off-axis aberration so that the rays are admitted to the effective area of the infrared detector uniformly. A prototype of an infrared gas detector was produced with the designed optical cavity to confirm the performance.

Keywords : Off-axis parabolic mirror, Non-dispersive infrared, Gas detector
OCIS codes : (040.3060) Infrared; (080.4035) Mirror system design

I. INTRODUCTION

A non-dispersive infrared (NDIR) gas detector is essential equipment for protecting lives and property against accidents due to toxic and inflammable gases included in the air [1, 2]. The infrared gas detector uses the property of gas that is composed of two or more different atoms and absorbs the infrared light at a unique wavelength for each atom [3]. It converts the differential in the amount of light caused by the infrared light absorption rate of the gas into gas density for measurement [4]. The absorption of the infrared light is expressed as the Beer-Lambert Law, Eq. (1) [5].

I_o [W/m^2] indicates the intensity of the light emitted from the infrared light source and I_d [W/m^2] indicates the intensity of the light going into the infrared light detector. K is the infrared light absorption coefficient of the specific gas, C is the density of the gas, and L is the length of the ray path between the infrared light source and the detector in the optical cavity [6]:

$$I_d = I_o \exp(-KCL). \quad (1)$$

According to Eq. (1), the infrared gas detector has less measurement error when the ray path, the course of the infrared light traveling from the light source to the optical detector, increases as more light is absorbed by the gas and the differential in the amount of light increases. In other words, having the maximum ray path in an optical cavity of the same size determines the performance of the infrared gas detector; therefore the optical design of the optical cavity of the infrared gas detector is essential. In general, a method of increasing the optical path through the reflection of the gas cavity at a limited size using a concave structure is used, in which case off-axis aberration occurs. Therefore, an optical cavity design of a parabolic structure is required to eliminate off-axis aberration.

This study designed an optical cavity which converts the infrared light emitted from the light source into parallel light using the off-axis parabolic mirror to easily secure a long ray path and increases the ray path through multiple reflections. A prototype of an infrared gas detector was produced based on the optical cavity designed with the goal of achieving 5% or higher measurement sensitivity

*Corresponding author: msoptic@kpu.ac.kr, ORCID 0000-0003-3430-876X
Color versions of one or more of the figures in this paper are available online.

differential when detecting 500 ppm of CH_4 gas and 1,000 ppm of CO gas [7].

II. DISCUSSION AND METHODS

2.1. Light Source

A gas molecule absorbs the light of a specific wavelength as shown in Table 1 [8]. The light source used in the gas detector in this study was EMIRS200_R_60/55_0 (TO39 with Reflector1) IR source by Axetris in Fig. 1(a). It can be applied to various active target gases that react to infrared light as it has 2 μm or greater broad band of release wavelength as shown in Fig. 1(b). Also, the IR source had high power and small divergence angle, which allowed easier designing of an optical cavity than for that with an LED light source [9]. Detailed specifications of this light source are shown in Fig. 1(c).

2.2. Detector

The detector used in this study was manufactured by InfraTec, and has two channels as shown in Fig. 2(a). Each channel has the advantage that it can simultaneously detect different kind of gases using the optical filter that lets through the wavelength band in a specific range [10]. The two light filters can selectively detect two different gases because each can select a different spectrum channel.

TABLE 1. Absorption lines of gas

Gas	Absorption lines (um)
H_2O	2.5~2.8
C_2H_2	3.0~3.1
CH_4	3.2~3.45
H_2CO	3.4~3.7
HBr	3.7~4.0
SO_2	4.0
CO	4.2~4.3

Dual light filters also have a low channel crosstalk of less than 0.1%, resulting in low error when measuring mixed gases. The detectivity is 2.5E + 08 cm (sqrt[Hz])/W.

Also, the detector consumes less power and enables accurate detection regardless of the changes in the atmosphere as it has a temperature compensation system against absorption wavelength of the gases that change according to temperature changes. The detector has FOV as shown in Fig. 2(b) and the angle of the light coming into the detector shall be 22.5° or less.

2.3. Coating Material

The infrared gas detector uses multiple reflecting surfaces inside the optical cavity to secure a long ray path, and the reflection rate of the reflecting surface becomes an important factor for the performance of the gas detector.

Figure 3 shows the reflection rate by wavelength in the infrared light according to the coating material [11].

Gold, silver, aluminum, and copper, which are industrial coating materials that can be used in the IR area, were selected to reduce the loss of light by reflection in the area of 2,000 nm or greater infrared light, which is the wavelength used by the infrared gas detector. Gold, which does not corrode and does not cause changes in the reflection rate, was selected as the coating material.

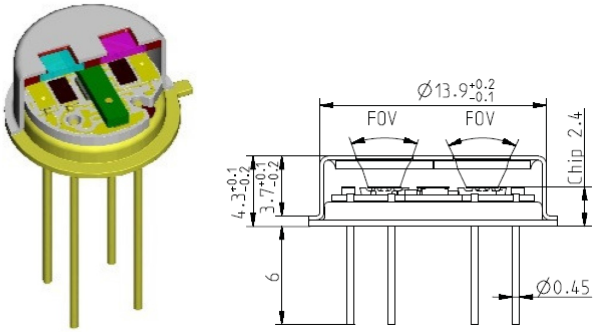

(a) (b)

FIG. 2. Detector (a) Detector shape, (b) Detector side view.

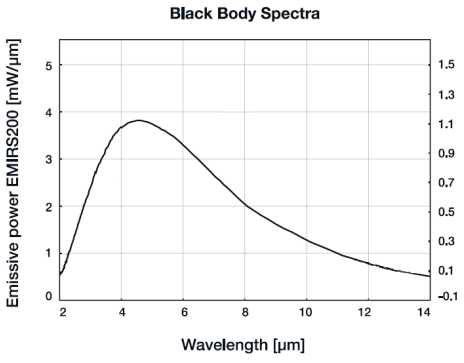

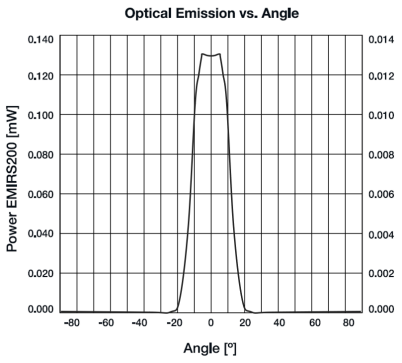

(a) (b) (c)

FIG. 1. IR source (a) EMIRS200 IR source, (b) Wavelength band graph and (c) Light distribution.

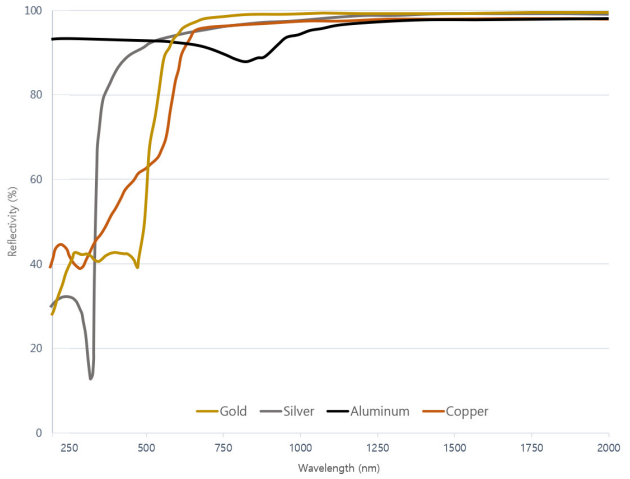

FIG. 3. Coating material reflectivity.

The gold plating has advantages, such as high infrared light reflection rate and solid coating. However, it is difficult to apply a thick coating due to the high price. The reflection rate is 95% with the ordinary plating thickness of 0.33 μm, and the actual reflection rate is estimated to be lower considering the uneven surface of the optical cavity. Considering this fact, the reflection rate of the 0.33 μm gold plating was set to 92% in the design.

2.4. Design of Optical Cavity

2.4.1. Basic setting and first mirror

The design was implemented within the optical cavity sized 70 mm × 40 mm × 15 mm (L × W × D). Figure 4(a) shows the form of the optical cavity and the location of the light source and the detector.

After the light emitting from the light source turns into a parallel line through the first mirror, the ray path can be easily controlled. However, tilting the first mirror to increase the length of the ray path will cause off-axis aberration due to the characteristics of the reflecting optical system. To resolve this problem, the off-axis parabolic mirror shown in Fig. 4(b) was used.

The off-axis parabolic mirror only uses the off-axis area, which is off the axis of the ordinary optic axis parabolic mirror, and it parallelizes the central beam of the light source that travels in off-axis, not parallel to the optic axis of the parabolic mirror.

In other words, the optic axis parabolic mirror must be designed first before designing the off-axis parabolic mirror. Equation (2) is the parabolic equation. The focal distance F of the optic axis parabolic mirror was set to 32 mm considering the size of the optical cavity, 70 mm × 40 mm × 15 mm (L × W × D), and the distance between the light source to the first mirror, and a parabola was derived as seen in Fig. 4(c):

$$x^2 = 4 \cdot Fy \rightarrow x^2 = 128y. \quad (2)$$

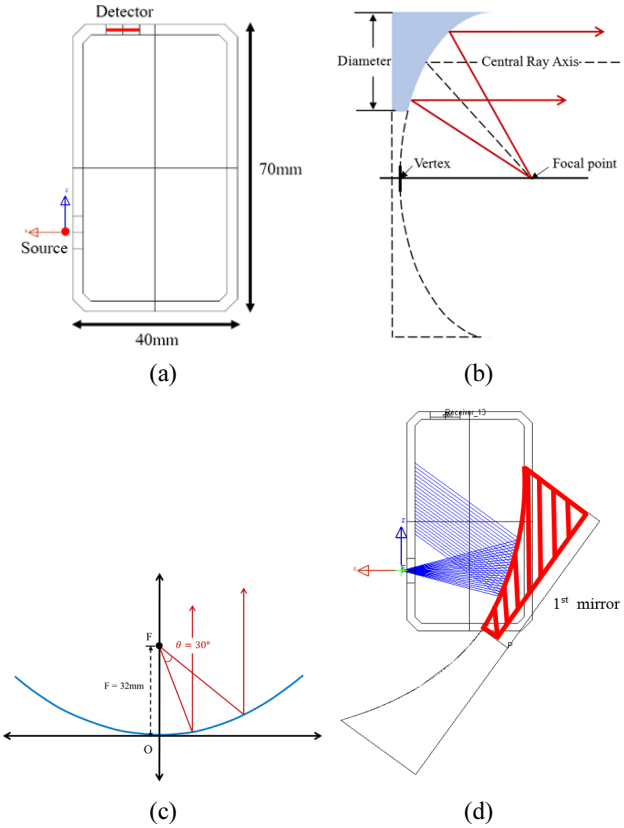

FIG. 4. Basic setting and first mirror (a) Schematic of optical cavity, (b) Off-axis parabolic mirror and (c) Parabolic graph and 1st reflector (off-axis parabolic mirror).

Figure 4(d) shows the off-axis parabolic mirror which uses a part of the parabolic mirror in Fig. 4(c). It shows that the light emitted from the light source travels in parallel through the first mirror, the off-axis parabolic mirror.

2.4.2. Second mirror

The beams reflected off the first mirror are parallel and the flat mirror is used inside the optical cavity.

The beam width of the parallel beams must be calculated in order to set the size of the flat mirror after the first mirror. The beams that travel along the ray path travel in parallel after the first mirror and have a fixed beam width. The two points, at which the beams diverted at the angle of 30° to meet the off-axis parabolic mirror, were derived by using the parabolic Eq. (2) to calculate the width of the beams reflected off the first mirror as shown in Fig. 5(a).

The points at which the beams corresponding with +15° and -15° at light source F meet the parabolic mirror are A (37.9, 10.2) and B (32.0, -8.6), respectively. The distance between A and B and the angle of the x axis, θ, can be calculated with Eqs. (3) and (4) using the equation of the straight line which connects two points:

$$\overline{AB} = \sqrt{(38-32)^2 + (10+9)^2} \cong 19.7\ \mathrm{mm}, \quad (3)$$

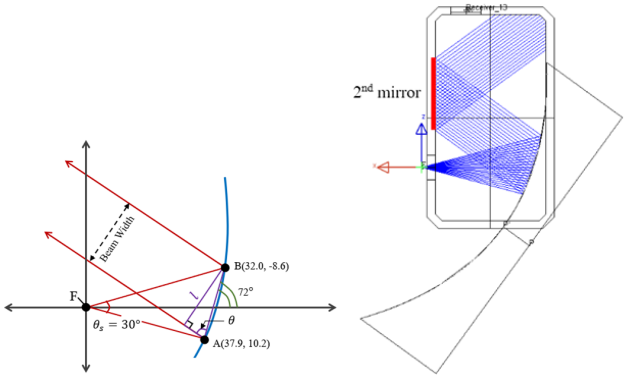

(a) (b)

FIG. 5. Second mirror (a) Beam width reflected from the 1st parabolic mirror, (b) 2nd mirror.

$$\theta = \tan^{-1}\left(\frac{10.2+8.6}{37.9-32.0}\right) \cong 72°. \quad (4)$$

The beam width calculated with Eq. (5), using the central optic axis of the parabolic mirror and the divergent angle of the light source, comes to 18.7 mm:

$$l = 19.7 \times \sin(180° - 72° - 36°) = 18.7\,\mathrm{mm}. \quad (5)$$

The second reflecting surface is in the front side of the detector and tilting this surface would block the beams coming into the detector. It was placed in the same angle as the wall of the optical cavity so as not to block the ray path, as shown in Fig. 5(b).

2.4.3. Third mirror

Since the beams reflecting off the second flat mirror will continue to travel in parallel, the width of the beams going to the third and fourth mirrors will also be 18.7 mm. The mirror was designed at 22 mm, 20% larger than the beam width, to take all beams coming in.

As the beams reflecting off the third mirror move toward the fourth mirror and the beams off the fourth mirror enter the detector, the entire ray path is completed. The detector has FOV, and the beams reflecting off the fourth mirror must enter the detector nearly perpendicularly. The angle of the third mirror was designed based on the law of reflection so that the fourth mirror can be located at the point on which the foot of perpendicular was drawn from the center of the detector as shown in Fig. 6.

2.4.4. Fourth mirror

The beams reflecting off the fourth mirror will enter the detector which has two channels as shown in Fig. 7. The sensitivity of the detector indicates the output per input, and more input signal will result in higher output, which will facilitate signal processing in the following stage. The beams must be concentrated on the effective area of the detector in order to achieve the maximum light efficiency of the detector [12].

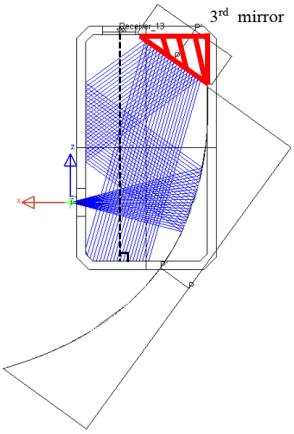

FIG. 6. 3rd mirror.

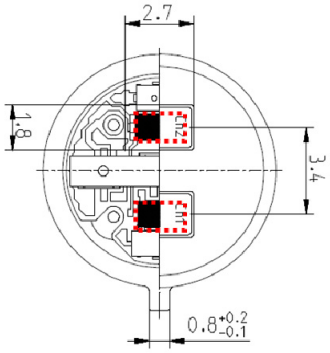

FIG. 7. Effective area of the detector.

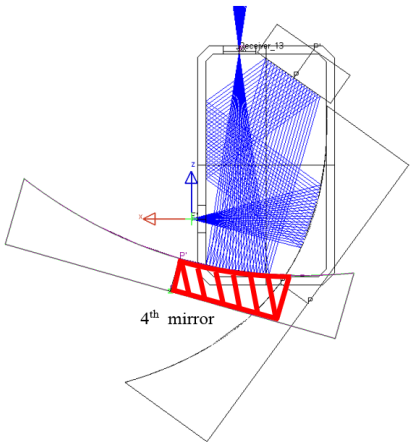

FIG. 8. 4th parabolic mirror.

Like the first mirror, an optic axis parabolic mirror with a focal distance of 63 mm was designed considering the size of the entire optical cavity, distance between the fourth mirror and the detector, and the effective area of the detector. The off-axis parabolic mirror, which used a part of the designed optic axis parabolic mirror, was used as the fourth mirror and its image is shown in Fig. 8.

The simulation was created using the optical design program, LightTools. Figure 9 shows the result of simulating of the illumination of light that entered the receiver after the first, second, third, and fourth mirrors. Figure 9(b) shows the result of the simulation using the on-axis parabola. Figure 9(a) shows the result when two off-axis parabolic mirrors are used to correct off-axis aberration. As a result, in contrast to Fig. 9(b), they concentrated the light in the effective area of the detector, forming symmetry and uniformly condensing the light in the middle of the receiver.

Figure 10 shows the overall layout of the designed gas sensor, indicating the location of the light source, detector, and the hole through which the gas passes in and out.

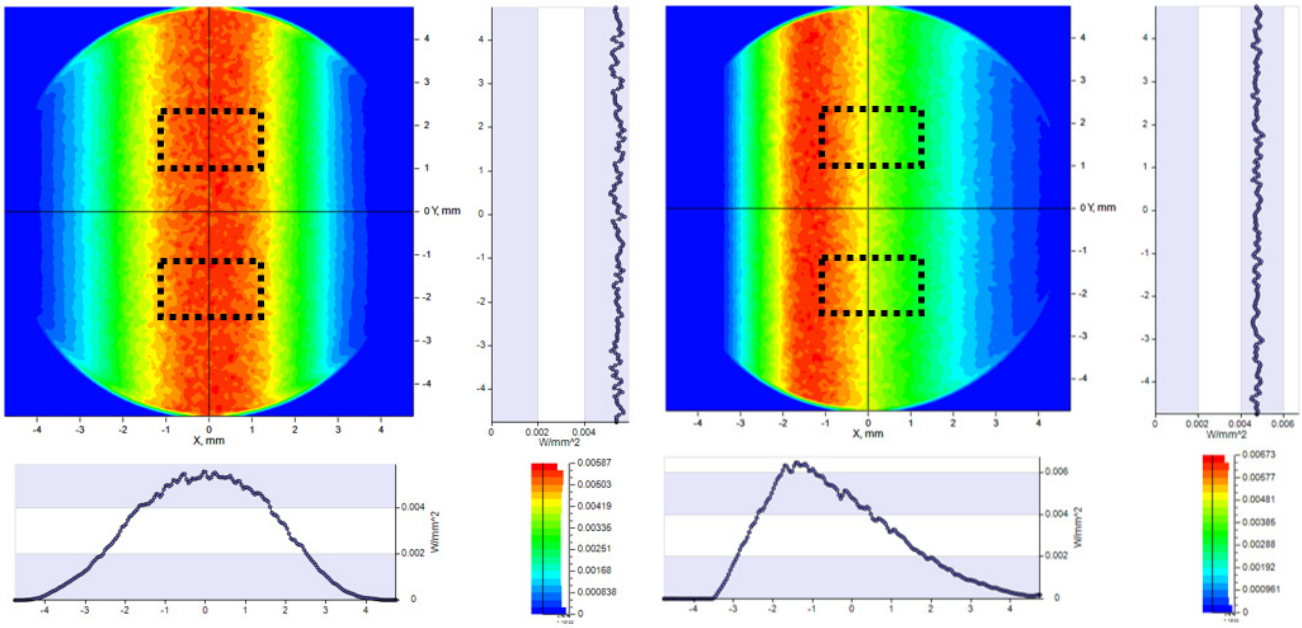

(a) (b)

FIG. 9. Results of illumination simulation and effective area of the detector (a) Results of illumination simulation when using off-axis parabola, (b) Results of illumination simulation when using on-axis parabola.

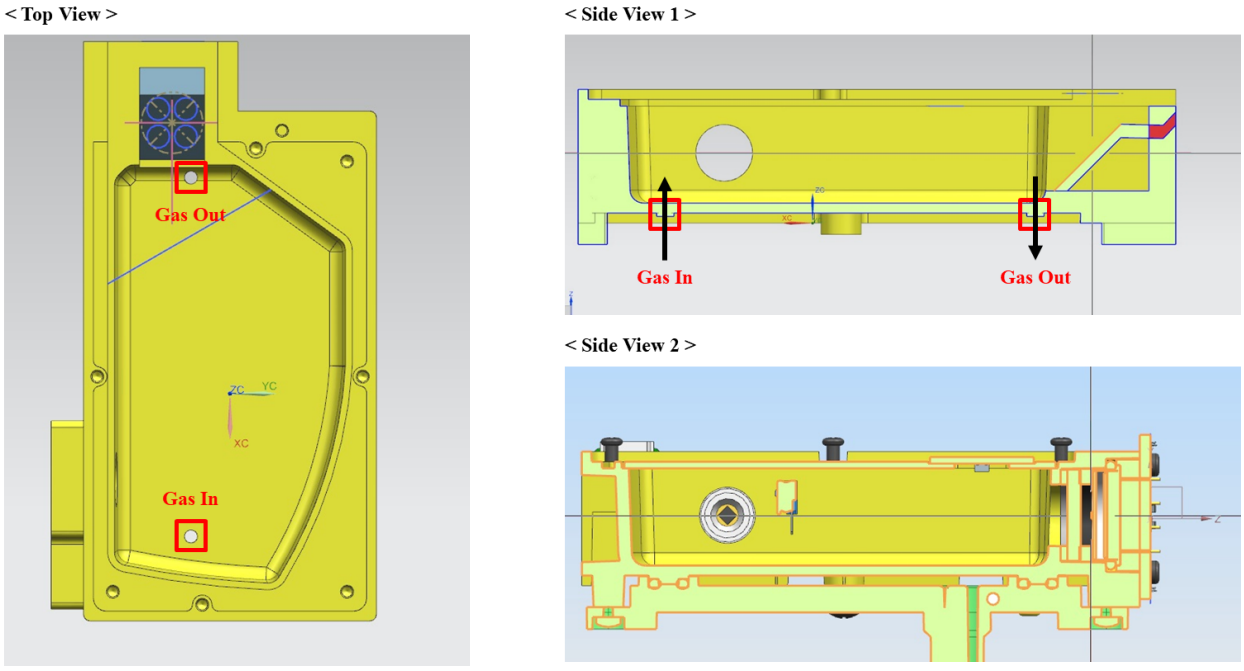

FIG. 10. Overall layout of the designed gas sensor.

III. RESULTS

3.1. Analysis of Ray Path

According to Eq. (1) Beer-Lambert Law, the ray path is an important factor for enhancing the accuracy of the infrared gas detector. The ray path especially becomes more important as gas with a lower optical absorption rate has smaller signals entering the detector.

The ray path in which the light sequentially reflected off the first, second, third, and fourth mirrors through the optical design before entering the detector is defined as the "intended ray path" and other paths "unintended ray path."

Rays coming through paths shorter than the intended ray path have less light absorbed by the gas and may deteriorate the accuracy of the analysis results while rays coming through longer paths will lose intensity and do not affect the results. In other words, it is necessary to analyze the ray path to determine whether the beams of the designed optical cavity travel through the intended ray path. Figure 11 illustrates the straight ray path where the light is reflected off the first through fourth mirrors sequentially before it enters the detector.

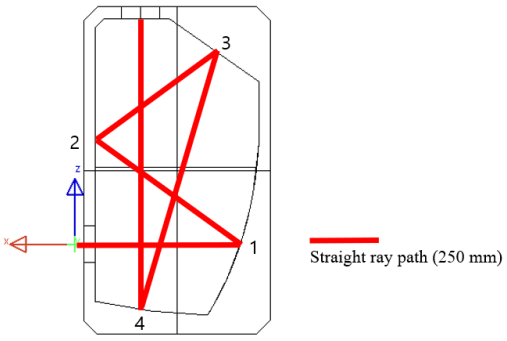

FIG. 11. Straight ray path.

The length of the straight ray path from the light source to the detector is 250 mm. Figure 12(a) shows the optical paths of 300 beams randomly emitted from the light source, Fig. 12(b) shows the beams among the 300 that move in the intended ray paths, and Fig. 12(c) shows the beams that move in unintended ray paths.

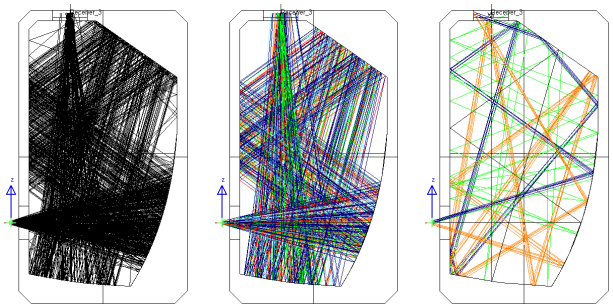

(a) (b) (c)

FIG. 12. Analysis of the ray path (a) Exemplary ray paths of 300 rays, (b) Desired rays and (c) Undesired rays.

Figure 13(a) shows the number of beams with ray paths of 245~255 mm (- intended ray path -) among the 300 random beams and the number of beams with unintended ray paths, indicating that over 96% of the 300 beams travelled through the intended ray path [13]. Figure 13(b) is a graph that shows the ratio of intended ray paths and unintended ray paths through a simulation of 50,000,000 beams. This shows that 98.6% of the amount of light that entered the receiver was effective.

As the gas detector's accuracy increases when the amount of light coming in unintended ray paths is small, a ray path analysis was performed, and it confirming that the design is reliable.

3.2. Production and Measurement

A prototype of the optical cavity was produced based on the verified reliable design through the ray path analysis. Figure 14 shows the optical cavity produced by depositing 0.33 μm of gold on the inner reflecting surface.

Figure 15(a) shows the driving unit of the infrared gas detector. The driving unit amplifies the voltage flowing

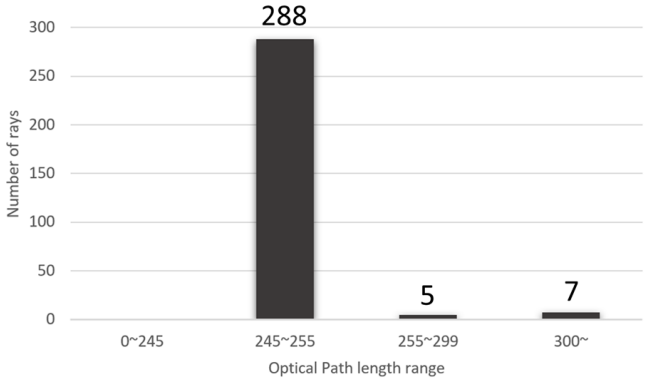

(a)

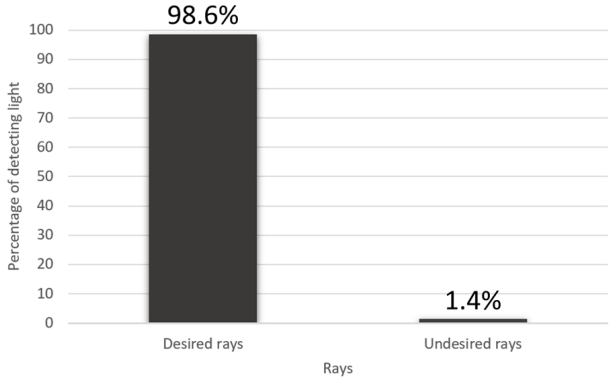

(b)

FIG. 13. Analysis of the desired rays (a) Ray path length distribution versus the number of rays, (b) Percentage of light.

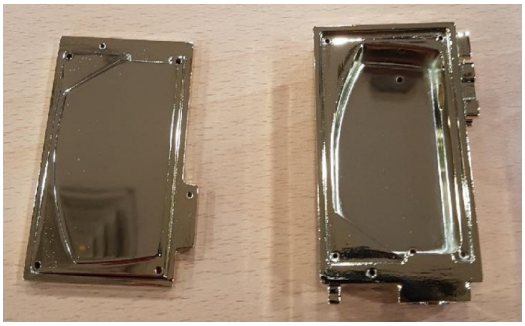

FIG. 14. Optical cavity.

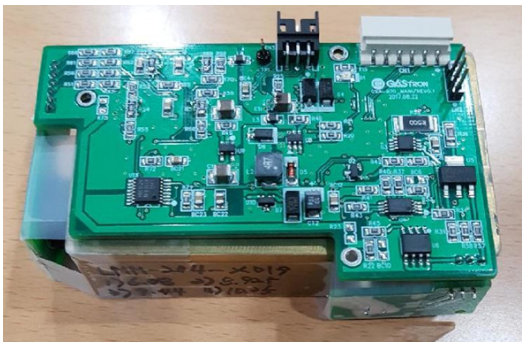

FIG. 15. Diving part of NDIR gas detector.

into the detector in a uniform and stable voltage through the amplifier and eliminates noise using the low pass filter to facilitate accurate measurement.

Figure 16(a) shows standard deviation with set CH_4 gas concentration for temperature 25°C and relative humidity 50%. Figure 16(b) shows a linearity graph of the gas detector designed and manufactured. This is the data on CO_2 gas, which shows that it shows excellent linearity. The detection range of the gas detector is 0~10,000 ppm/1.0%.

CH_4 and CO gas detection test was performed respectively with the prototype. The changes in the output voltage were measured with 500 ppm of CH_4 gas and 1,000 ppm of CO gas when the room temperature was 25°C and relative humidity 50%.

Figure 16(a) shows the result of measuring CH_4 gas. The measurement voltage of the detector changed from 1.065 V to 1 V, showing approximately 6.1% of measurement voltage differential when detecting with 500 ppm of CH_4 gas. Figure 16(b) shows the result of measuring CO gas. The measurement voltage of the detector changed from 2.08 V to 1.95 V, showing approximately 6.25% of measurement voltage differential when measuring with 1,000 ppm of CO gas. Both types of gases satisfied the intended measurement sensitivity differential of 5% or higher.

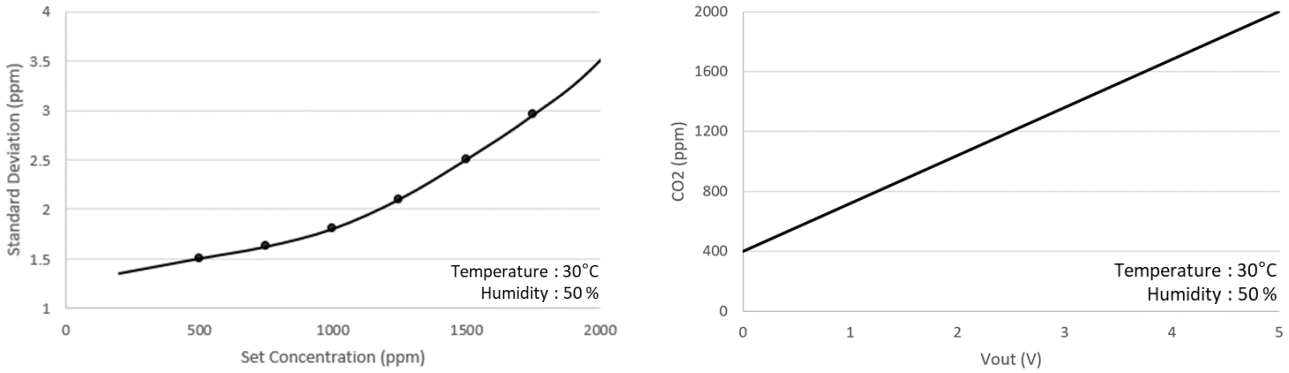

(a) (b)

FIG. 16. Specification of gas detector (a) Measured standard deviation, (b) Linearity of the gas detector on CO_2.

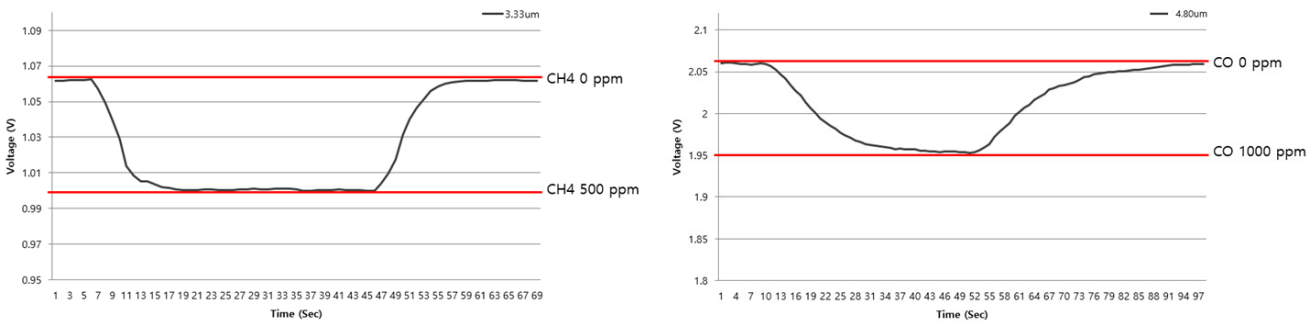

(a) (b)

FIG. 17. Measurement result of gas (a) CH_4 gas 500 ppm test, (b) CO gas 1000 ppm test.

IV. CONCLUSION

This study examined the optical cavity design of the non-dispersive infrared gas detector. Since the infrared gas detector has less measurement error when the ray path from the source of infrared light to the detector is greater, a design that involves a long ray path is required. However, designing the detector using multiple reflecting surfaces to increase the length of the ray path causes off-axis aberration due to the characteristics of the reflecting optical system.

To eliminate this problem, the design incorporated off-axis parabolic mirror to parallelize the light to easily achieve a long ray path and eliminate off-axis aberration, letting the light uniformly enter the effective area of the infrared detector. As a result, an optical cavity with 250 mm long ray path using two off-axis parabolic mirrors and two flat mirrors was designed, and the analysis of the optical cavity design proved its reliability with intended and unintended ray paths, accounting for 98.6% and 1.4% of the amount of light, respectively.

The designed optical cavity was fabricated and the standard deviation according to the set concentration was measured. The prototype prepared based on the analysis results showed a measurement sensitivity differential of 6.1% when measuring 500 ppm of CH_4 gas and 6.25% when measuring 1,000 ppm of CO gas, achieving the measurement sensitivity differential of 5% or greater.

ACKNOWLEDGMENT

This work was partly supported by the Educational Research Promotion Program in year 2018 of Korea University of Technology and Education.

REFERENCES

1. L. Jun, T. Quilin, Z. Wendong, X. Chenyang, G. Tao, and X. Jijun, "Miniature low-power IR monitor for methane detection," Measurement **44**, 823-831 (2011).
2. G. Zhang, Y. Li, and Q. Li, "A miniaturized carbon dioxide gas sensor based on infrared absorption," Opt. Lasers Eng. **48**, 1206-1212 (2012).
3. J. Hodgkinson and R. P. Tatam, "Optical gas sensing: a review," Meas. Sci. Technol. **24**, 012004 (2012).
4. S. H. Yi, J. S. Park, and D. G. Lee, "The characteristics of concaved optical cavity structure with focusing effect of infrared light," in *Proc. The Korean Institute of Gas Spring Conference* (Ramada Plaza Jeju, Korea, Apr. 2009), pp. 190-194.
5. D. S. Vlachos, P. D. Skafidas, and J. N. Avaritsiotis, "The effect of humidity on tin-oxide thick-film gas sensors in the presence of reducing and combustible gases," Sens. Actuators, B **25**, 491-494 (1995).
6. J. H. Kim and C.-J. Lee, "Three - harmful gas detection sensor module using non-dispersive infrared (NDIR) technology," J. Korean Inst. Commun. Inf. Sci. **42**, 1591-1598 (2017).
7. S. H. Yu, S. H. Yi, K. H. Kwon, and N. K. Min, "Design of novel optical cavity for NDIR gas sensor with high output power," in *Proc. KIEE Conference* (Yongpyong Resort, Korea, Jul. 2006), pp. 1641-1642.
8. G. T. Park, "A study on the measurement accuracy improvement of a portable combustible gas detector using an infrared sensor," Ph. D. *Thesis*, University of Seoul, Seoul (2014), pp. 1-168.
9. S. H. Yi and J. S. Park, "Speculation of optical cavity for improving optical gas sensor's characteristics," J. Korean Inst. Gas **12**, 63-68 (2008).
10. K. Laqua, B. Schrader, G. G. Hoffmann, D. S. Moore, and T. Vo-Dinh, "Nomenclature, symbols, units and their usage in spectrochemical analysis-XI. Detection of radiation (IUPAC Recommendations 1995)," Pure Appl. Chem. **67**, 1745-1760 (1995).
11. B. Wang and L. Gallais, "A theoretical investigation of the laser damage threshold of metal multi-dielectric mirrors for high power ultrashort applications," Opt. Express **21**, 14698-14711 (2013).
12. J. S. Park, H. C. Cho, and S. H. Yi, "Simulation of optical cavity for improving the light intensity," in *Proc. The Korean Institute of Gas Spring Conference* (Seoul Technopark in Seoul National University of Science and Technology, Korea, Apr. 2008), pp. 164-169.
13. I. Sieber, H. Eggert, K.-H. Suphan, and O. Nuessen, "Optical modeling of the analytical chamber of an IR gas sensor," Proc. SPIE **4408**, 272-282 (2001).